Quasi-self-similarity for wetting drops

R. Gratton, J. A. Diez, L. P. Thomas, B. Marino, and S. Betelú
Instituto de Física Arroyo Seco, Facultad de Ciencias Exactas, Universidad Nacional del Centro de la Provincia de Buenos Aires, Pinto 399, 7000 Tandil, Argentina
(Received 3 March 1995)

We develop and experimentally test a quasi-self-similar solution for the spreading of viscous nonvolatile droplets over a dry and horizontal solid substrate, under the condition of complete wetting (spreading parameter $S > 0$) with both gravity and Laplace pressure as driving forces. The problem does not admit a self-similar solution because two dimensional characteristic parameters, namely, the slipping length λ and the capillary distance a, cannot be ruled out. Therefore, we approximate the solution by the members of a family of self-similar solutions, each one corresponding to different values of the ratios x_f/a and h_0/λ, where x_f and h_0 are the instantaneous drop extension and central thickness, respectively. This treatment of the problem also produces an explicit formula (which must be integrated) to predict the drop radius. The excellent agreement with our own and other authors' experimental data suggests that the approach can be considered as an interesting tool for solving problems where strict self-similarity fails.

PACS number(s): 47.15.Gf, 47.10.+g, 68.45.Gd, 68.10.Cr

I. INTRODUCTION

Recently, attention has been devoted to the spreading of viscous drops over a completely wettable horizontal substrate, with both gravity g and surface tension γ at the drop free surface as the driving forces. Gravity is the main driving force [1–3] when the volume V is large, i.e., $V^{1/3} > a$, where $a = \sqrt{\gamma/\rho g}$ is the capillary length and ρ the liquid density ($a \cong 1.5$ mm for the liquids currently used in experiments); on the contrary, when the volume is small, the gradient of the Laplace pressure dominates [4–9]. However, a more detailed analysis shows that the regimes in which one of these forces prevails cannot be sharply separated. For instance, when the radius of a drop greatly exceeds a, experiments [10–13] show that gravity becomes important. On the other hand, when the thickness of a large drop becomes of the order of a, the surface tension produces small but appreciable effects [14]. This situation arises because the ratio between both forces is spatially nonuniform: gravity prevails in the central region of the drop and Laplace pressure prevails near the edge [12].

Unfortunately, the application of self-similarity methods, useful to simplify the description of flows with simple symmetries, encounters here serious troubles. The first difficulty is that realistic boundary conditions at the drop edge break self-similarity [15] because they introduce characteristic lengths (or other dimensional parameters) related to local microscopic scales, independent from those describing the macroscopic scale. As the microscopic mechanisms by which a liquid wets a solid are not yet sufficiently known, the formulation of reliable boundary conditions is an open problem. However, all reasonable choices exhibit the previous shortcoming. Here we adopt the usual slipping approach [16–24], which consists of the relaxation of the no-slip boundary condition at the liquid-solid interface by the introduction of a slipping length λ. Under this assumption it is possible to put the thickness at the drop edge (front) to zero without leading to the divergence of the viscous dissipation rate and thus avoiding the contact line paradox [25,26]. The second difficulty is that when both gravity and surface tension are considered, another characteristic length appears, namely, the above mentioned capillary length a.

The current way to overcome these difficulties is to divide the flow into two or more spatial regions where gravity or alternatively Laplace pressure is dominant [12,13,18]; then, the complete solution is obtained by matched asymptotic expansions between both regions. An example of this kind of approach is the solution given by Hocking [18] to the problem of partially wetting drops spreading. These models, as well as the approach presented here, use the lubrication approximation theory and also concern the intermediate asymptotic regime, where the particularities of the initial conditions are irrelevant.

In this work, we extend an approach developed in a previous paper [15], in which gravity was neglected but nevertheless self-similarity was broken due to the first difficulty mentioned above. An analogous idea (called local similarity) was also used to describe the boundary layer flow on a flat plate with uniform suction or injection [27] and also in a nonlinear diffusion problem with an in-flow boundary condition [28]. The present method consists of building a solution (called the quasi-self-similar solution) that, at every instant, is approximated by the self-similar solution corresponding to the instantaneous values of the parameters $\Lambda = \lambda/h_0(t)$ (fractional slipping length) and $B = [x_f(t)/a]^2$ (Bond number), where $h_0(t)$ is the thickness at the center of the drop and $x_f(t)$ the front position. The members of this Λ and B dependent family of self-similar solutions extend spatially from the center ($x = 0$) to the drop edge ($x = x_f$), thus including regions with

 ©1996 The American Physical Society

quite different ratios between gravity and Laplace forces.

In Sec. II we describe the main features of the method and we show that the measured thickness profile of an actual spreading drop at time t agrees well with the profile given by the corresponding self-similar solution, i.e., the solution identified by the values of Λ and B for the drop at that time. At a successive time, the profile is given by another member of that family of solutions as Λ and B vary with time. Therefore, the flow is quasi-self-similar, as it is described by a succession of self-similar solutions, in analogy with the case of quasisteadiness. The main difference is that the self-similar solutions include the rate of variation of the magnitudes; as a result, we obtain the flow evolution without extra conditions. In Sec. III we show that this method provides a unified description of spreadings from $x_f \ll a$ (the Laplace limit) up to $x_f \gg a$. In Sec. IV we show that the time evolution of measurable magnitudes such as x_f, h_0, and the apparent contact angle θ_i agree very well with experiments.

II. QUASI-SELF-SIMILAR APPROACH

We simplify the Navier-Stokes equations by employing the well known lubrication approximation [Reynolds number $\mathrm{Re} = (\rho x_f v_f/\mu)(h_0/x_f)^2 \ll 1$, where μ is the fluid viscosity and $v_f = dx_f/dt$ is the front velocity]. By imposing the slipping boundary condition $v_x = \lambda\,(\partial v_x/\partial z)$ at $z = 0$ (x and z are the horizontal and vertical coordinates, respectively, and λ is a constant length), the z-averaged horizontal velocity $v = \langle v_x \rangle$ results

$$v = -\frac{\rho g}{3\mu} h\,(h + 3\lambda)\left(\frac{\partial h}{\partial x} - a^2 \frac{\partial c}{\partial x}\right), \tag{1}$$

where $h = h(x,t)$ is the drop thickness and

$$c = \frac{\partial^2 h}{\partial x^2} + \frac{\alpha}{x}\frac{\partial h}{\partial x} \tag{2}$$

is the local curvature with $\alpha = 0, 1$ for plane (ribbon) and axisymmetric (drop) symmetry, respectively. Both v and h satisfy the continuity equation, which, within the same approximation, reads

$$\frac{\partial h}{\partial t} + x^{-\alpha}\frac{\partial}{\partial x}\left(x^\alpha v h\right) = 0. \tag{3}$$

Equations (1)–(3) describe the time evolution of a drop spreading and are solved under the symmetry conditions

$$\frac{\partial h}{\partial x} = \frac{\partial^3 h}{\partial x^3} = 0, \quad x = 0, \tag{4}$$

the conditions at the contact line ($x = x_f$)

$$\begin{aligned} h &= 0, \\ \partial h/\partial x &= 0, \end{aligned} \tag{5}$$

and the volume conservation

$$V = \int_0^{x_f} (2\pi x)^\alpha\, h(x,t)\, dx = \text{const.} \tag{6}$$

The condition of zero slope at the front is a natural extension to this case of the condition proposed for partial wetting in which the static contact angle determines $\partial h/\partial x$ at $x = x_f$ [18]. Note that as the slope vanishes both at the center and at the front, an inflection point must exist in the thickness profile. The (maximum) slope at this point is referred to as the apparent contact angle θ_i.

As anticipated in the Introduction, a self-similar solution cannot be proposed because of the two characteristic lengths (not related to the initial conditions) involved in the problem, namely, the capillary length a and the slipping length λ. Therefore, we look for a solution that is successively approximated by the members of a family of self-similar solutions, each one corresponding to given values of the ratios Λ and B. Our guess is that the solution may be written as

$$\begin{aligned} h(x,t) &= h_0(t) H(\eta;\Lambda,B), \\ v(x,t) &= v_f(t) U(\eta;\Lambda,B), \end{aligned} \tag{7}$$

where $H(\eta;\Lambda,B)$ and $U(\eta;\Lambda,B)$ are nondimensional functions of $\eta = x/x_f$. Strictly, we should have written an explicit dependence on t, i.e., $H(\eta,t)$ and $U(\eta,t)$, but we suppose that they vary with time only as a consequence of the variation of Λ and B. Physically, this is reasonable if the characteristic diffusion time τ_{diff} ($\approx \rho x_f^2/\mu$) of the velocity field is much smaller than the evolution time of the dynamic parameters. Since a and λ are fixed, this time is approximately $t \approx x_f/v_f$. The existence of such a relation between τ_{diff} and t is the key point at the basis of the quasi-self-similar approach and is guaranteed in our case by the condition $\mathrm{Re} \ll 1$.

The extreme cases $g = 0$, $\gamma \neq 0$ and $g \neq 0$, $\gamma = 0$ merit some comments. In the first case, the equations do not admit self-similar solutions, in spite of the fact that they do not contain the capillary length; the boundary conditions given by Eq. (5) are the same than in the complete problem and therefore the slipping length λ must be maintained. The second case needs clarification. It is well known that a self-similar solution [1–3] exists when only gravity drives the spreading. However, this "pure gravity solution" is not the regular limit of the complete problem for $x_f \gg a$. In fact, it corresponds to a two orders lower differential equation obtained from Eq. (1) by setting both $a = 0$ and $\lambda = 0$; the only boundary condition at x_f required to build up the solution is $h(x_f) = 0$ and, as a result, $\partial h/\partial x \to \infty$ there. This last feature, clearly not compatible with the second condition of Eq. (5), is essential to allow for $\lambda = 0$. Instead, the limit of the complete problem leads to a qualitatively different profile of the front region because $h(x,t)$ has to match both conditions of Eq. (5). However large the ratio x_f/a is, there is a peripheral region dominated by capillarity, where the slope goes to zero after an inflection point, so that λ cannot be ruled out from Eq. (1). The width of this region is of the order of a, thus the fraction of the drop affected by capillarity decreases as a/x_f. Of course, as gravity prevails throughout all the remaining flow, the profile tends to the pure gravity profile as $x_f/a \to \infty$, except for this peripheral region. Clearly,

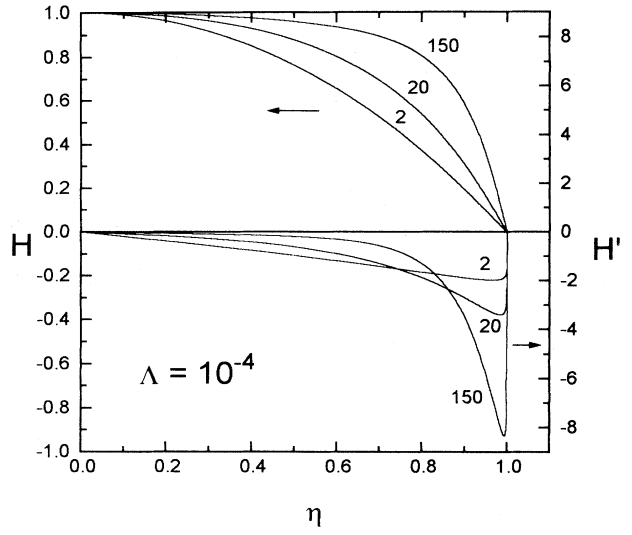

FIG. 1. $H(\eta)$ and $H'(\eta)$ obtained from Eq. (16) for $\Lambda = 10^{-4}$ and $B = 2, 20, 150$.

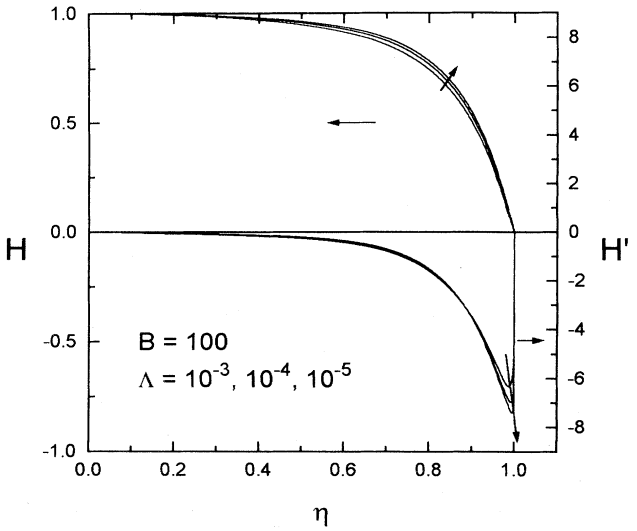

FIG. 2. $H(\eta)$ and $H'(\eta)$ obtained from Eq. (16) for $B = 100$ and $\Lambda = 10^{-3}$,10^{-4},10^{-5}.

this limit is not strictly self-similar.

By replacing Eq. (7) into Eqs. (1) and (3) we obtain the ordinary differential equations

$$\beta U = H\,(H + 3\Lambda)\,(C' - BH')\,, \tag{8}$$

$$\omega H - \eta H' + \eta^{-\alpha}\,(\eta^{\alpha} U H)' = 0, \tag{9}$$

where the primes denote derivation with respect to η. Here we introduce the nondimensional curvature

$$C = H'' + \frac{\alpha}{\eta} H' \tag{10}$$

and the nondimensional parameters

$$\beta = \frac{3\mu}{\gamma} v_f \left(\frac{x_f}{h_0}\right)^3, \quad \omega = \frac{x_f}{v_f h_0}\frac{dh_0}{dt}. \tag{11}$$

An explicit dependence on t for H and U would result in an additional term of the form $x_f(\partial H/\partial t)/v_f$ in Eq. (9); the present approach requires it to be negligible with respect to the remaining terms.

In the variables defined by Eq. (7), the constant volume condition Eq. (6) reduces to

$$V = I h_0 x_f^{\alpha+1} = \text{const}, \tag{12}$$

where

$$I = \int_0^{x_f} (2\pi\eta)^{\alpha} H(\eta)\, d\eta \tag{13}$$

will be called hereinafter the "shape factor." Equation (12) implies that if dI/dt is zero or negligible, as would be the case if Λ and B were constants, we have

$$\omega = -(\alpha + 1). \tag{14}$$

Hence Eq. (9) admits the exact analytical solution

$$\eta^{\alpha} H(U - \eta) = \text{const}. \tag{15}$$

As this equation must be satisfied for $\eta = 0$ where $U = 0$, the constant on the right-hand side is zero; therefore, the solution of Eq. (15) is simply $U = \eta$, i.e., the velocity profile is linear. We assume that this property is retained even though I changes because of the variations of Λ and B. This assumption is based on the smallness of τ_{diff} with respect to the characteristic time t. This is equivalent to describing the flow instant by instant by a different self-similar solution, each one corresponding to the instantaneous values of Λ and B. This approximation was also used by Brochard-Wyart *et al.* [12].

In order to obtain these self-similar solutions, we must solve the third-order differential equation (8) with $U = \eta$, that is,

TABLE I. Values of the parameters obtained for $\Lambda = 10^{-4}$.

B	β	C_0	I
2	0.546	-0.368	1.602
20	2.909	-1.524	1.955
150	43.506	-0.596	2.454

TABLE II. Values of the parameters obtained for $B = 100$.

Λ	β	C_0	I
10^{-3}	31.72	-0.686	2.334
10^{-4}	25.33	-0.553	2.383
10^{-5}	21.07	-0.464	2.418

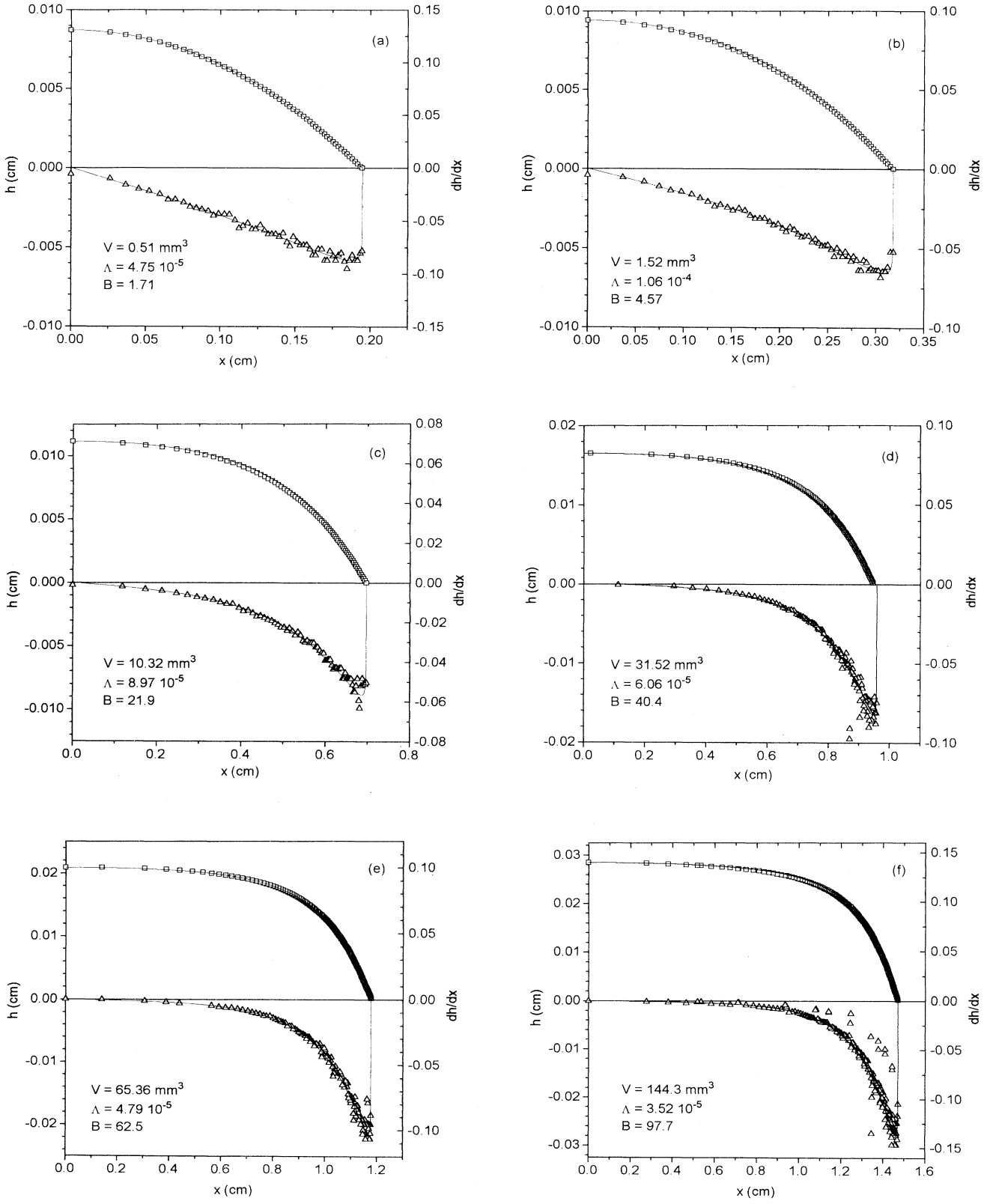

FIG. 3. (a)–(f) Comparison of the theoretical profiles (solid lines) with the experiments (symbols). The squares correspond to experimental values of h obtained by interferometry and the triangles to the numerical derivative of the h curves. For the theoretical calculations we have used $\lambda = 10^{-6}$ cm and all the cases correspond to $\mu = 10$ P, $\rho = 0.97$ g/cm^3, and $\gamma = 20.9$ dyn/cm.

$$\beta\eta = H\,(H + 3\Lambda)\,(C' - BH')\,, \tag{16}$$

with the boundary conditions

$$\begin{aligned} H(0) &= 1, \quad H'(0) = 0, \\ H(1) &= 0, \quad H'(1) = 0. \end{aligned} \tag{17}$$

Note that the condition $H'''(0) = 0$ is identically satisfied by Eq. (16). Here, these four conditions are sufficient to determine the solution of Eq. (16) including the value of β for given values of Λ and B. However, we need the values of β and $C_0 = (\alpha + 1)H'''(0)$ to integrate from $\eta = 0$; in order to calculate them consistently with the boundary conditions given by Eq. (17), we guess values of β and C_0 and then integrate numerically until $\eta = 1$. We use twice a bisection method: first, we adjust C_0 to obtain $H(1) = 0$ and, second, we iterate in β to achieve $H'(1) = 0$. In this way, we obtain the complete solution of Eq. (16) for every given pair of Λ and B.

In Fig. 1 we show $H(\eta)$ and $H'(\eta)$, respectively, for $\Lambda = 10^{-4}$and $B = 2$, 20, and 150 and in Table I we give the corresponding values of β, C_0 , and I. The thickness profile is quite sensitive to the value of B, the relevant feature being the flattening of the central region, which affects a larger fraction of the drop extension as B increases, thus leading to larger values of I, as shown in Table I. Note that for small B (e.g., $B = 2$) the profile is almost parabolic, as evidenced by the corresponding near-linear function $H'(\eta)$ in Fig. 1. The maximum of $H'(\eta)$ for this case is close to 2, which is the value for the spherical cap solution. Larger values of B lead to higher values of the maximum, compensated by lower values of the slope in the bulk [the average value of $H'(\eta)$ is one].

To illustrate the influence of Λ, we show in Fig. 2 three different profiles $H(\eta)$ and $H'(\eta)$, respectively, for $B = 100$ and $\Lambda = 10^{-3}$,10^{-4},10^{-5} and we give the corresponding values of β, C_0, and I in Table II . In spite of the large range of Λ, the effect of its variation on the profile as a whole (see, for instance, the value of I) is very small as only the maximum slope is slightly modified. More significant is the influence of Λ on β; as we shall see in Eq. (18) in Sec. III, the time evolution is sensitive to the ratio β/I^3, so that the value of Λ (more specifically, the choice of λ) produces appreciable effects on the rate of spreading.

A key point of this work is to verify that the above solutions are suitable to describe instantaneously the flow for a wide range of Λ and B by studying experimentally numerous spreadings of different volumes (see Sec. IV). Here we show a set of representative cases to be compared with the solutions of Eq. (16), in their dimensional form. Though the calculation only requires given values of Λ and B, to make possible this comparison it is necessary to adopt a value for λ, as the experiments yield h_0, x_f, and a. Throughout this work we take $\lambda = 10^{-6}$ cm as a reasonable slipping length (we shall return briefly to this point at the end of Sec. IV). In Fig. 3 we give the theoretical curves and experimental data corresponding to six pairs (Λ, B). The symbols of the $\partial h/\partial x$ curves were obtained by a numerical differentiation of the experimental profiles. Clearly, the comparison of the slopes constitutes a more severe test than the comparison of the profiles. The excellent agreement shown in Fig. 3 constitutes support for the central assumption of the present approach, namely, that the instantaneous flow at $t = t'$ is properly described by the self-similar solution corresponding to $\Lambda(t')$ and $B(t')$.

III. TIME EVOLUTION: THEORETICAL RESULTS

A remarkable point is that the above self-similar solutions not only give the spatial features of the flow but also provide the rate of variation of the front position without the need of any additional assumption. In fact, from Eq. (11) we have the front velocity as

$$v_f = \frac{\gamma V^3}{3\mu}\frac{\beta}{I^3}x_f^{-(3\alpha+6)}. \tag{18}$$

As β and I are obtained when solving Eq. (16) with known values of Λ and B, the numerical integration of Eq. (18) gives $x_f(t)$ and also $h_0(t)$ $(= V/Ix_f^{\alpha+1})$. Equation (18) is analogous to Eq. (55) of Brochard-Wyart *et al.* [12], who uses Tanner's law ($\theta_d^3 = 9L\mu v_f/\gamma$), where $\theta_d \approx \theta_i$ is the so-called dynamic contact angle instead of the slipping boundary condition. In this way, the length λ plays the role of the free parameter L involved in the above law. If the flow were strictly self-similar, then β and I would be constants, thus leading to the power law

$$x_f = \xi_s\left(\frac{\gamma V^3}{3\mu}t\right)^{1/(3\alpha+7)}, \tag{19}$$

where the prefactor $\xi_s = [(3\alpha + 7)\beta/I^3]^{1/(3\alpha+7)}$ is a constant of the order of unity. However, in the general case, the front position should be obtained through a numerical integration of Eq. (18). In each time step, β and I must be recalculated in terms of the updated values of Λ and B.

For the time integration we give the constants V, ρ, μ and chosse $x_f \ll a$ in order to start from a Laplace pressure dominated regime; thus we estimate the initial time as $t_0 = (3\mu x_f/\gamma V^3)^{1/10}$ [see Eq. (19), $\alpha = 1$]. By assuming that the shape factor is $I = \pi/2$ (spherical cap shape), from the values of $x_f(t_0)$ and V we obtain $h_0(t_0)$ and then $\Lambda(t_0)$,$B(t_0)$. We also tried with different values of t_0 and verified that the solution for $t \gg t_0$ (say, $t = 10t_0$) practically does not depend on the initial values of x_f, h_0, and t_0, a property of the self-similar solutions that also holds for the quasi-self-similar case.

In what follows we give some numerical results showing the transition between the Laplace pressure to the gravity dominated regimes for three typical volumes and $\lambda = 10^{-6}$ cm. In Fig. 4 we represent the behavior of x_f, h_0, I, and $H_i' = \tan\theta_i/(h_0/x_f)$, where θ_i is the angle at the inflection point or apparent contact angle, following the usual experimental terminology. Both for $x_f(t)$ and $h_0(t)$ [Figs. 4(a) and 4(b)] two different power laws fit the solution at earlier and later times. It is worth noting that

the corresponding exponents are slightly different from those of the extreme self-similar solutions. For instance, in the case of $x_f(t)$, the exponents are 0.104 and 0.131 instead of 1/10 and 1/8 [1,9].

The shape factor I is very close to $\pi/2$ for small x_f/a [early times, lower dashed lines in Fig. 4(c)], as expected for a spherical cap. When x_f/a increases (late times), I reaches a maximum and then tends to a constant close

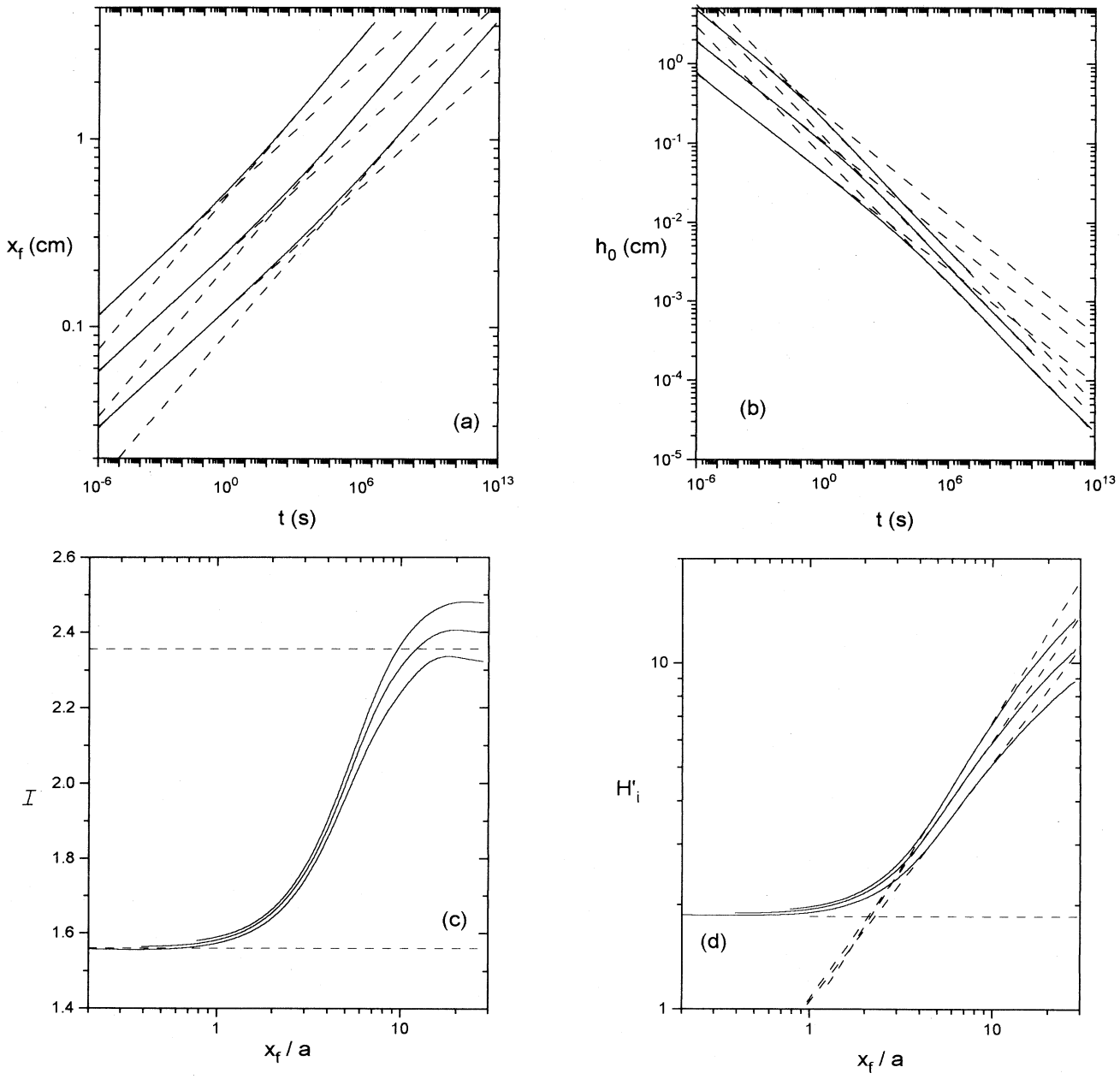

FIG. 4. (a) Front positions $x_f(t)$ calculated with the model (solid lines) for $\mu = 10$ P, $\rho = 0.97$ g/cm^3, and γ =20.9 dyn/cm, for $V = 1, 10$, and 100 mm^3, respectively (higher curves correspond to higher volumes). The power laws (dashed lines) that fit the solution have exponents 0.103,0.104,0.106 for the early times and 0.130,0.131,0.133 for the late times, respectively. (b) Thickness $h_0(t)$ at the center of the drop; the exponents of the power laws for early and late times are -0.206,-0.208,-0.215 and -0.270,-0.274,-0.277 for $V = 1, 10$, and 100 mm^3, respectively (higher curves correspond to higher volumes). (c) Volumetric shape factors I for $V = 1, 10$, and 100 mm^3 (higher curves correspond to higher volumes). The dashed lines correspond to $I = \pi/2$ and $3\pi/4$. (d) Ratio between the apparent contact angle and the aspect ratio $H_i' = \tan\theta_i/(h_0/x_f)$: the power laws that fit the solution for $5 < x_f/a < 10$ have exponents 0.691, 0.747, and 0.847 for $V = 1, 10$, and 100 mm^3, respectively (higher curves correspond to higher volumes). The horizontal line corresponds to $H_i' = 1.85$.

to but not coincident with the value corresponding to the $\gamma = 0$ self-similar solution [1], namely, $3\pi/4$ (higher dashed lines) and slightly dependent on V. In Fig. 4(d) we show H_i' as a function of x_f/a for the same cases. Clearly, for small x_f/a, $H_i' \cong 2$, showing again that the profile is virtually a spherical cap, while for large x_f/a, H_i' depends almost linearly on x_f/a, in agreement with a wedge shaped front region with slope $\tan\theta_i \cong h_0/a$ [12].

IV. TIME EVOLUTION: EXPERIMENTS

There is a considerable amount of published experimental results concerning viscous spreadings on wettable surfaces; however, relatively only a few may be used to critically test the time evolution given by the just developed quasi-self-similar solution. Most of the data concern the extreme regimes, where the Laplace pressure or, alternatively, the gravity is dominant. As a matter of fact, it is virtually impossible to observe in the same spreading an initial well defined Laplace pressure regime with $x_f < a$, then a transition stage, and, finally, a gravity dominated stage with $x_f \gg a$. In practice, the experimental study of the asymptotic intermediate spreading regime is limited to a time interval between a few seconds and about one day, which means a small part of the time variation range shown in Fig. 4(a). Therefore, the variation of x_f during a given spreading may hardly exceed half of a decade and the range of volumes for which $x_f \cong a$ at an intermediate stage is rather small. As a consequence, the changes in the flow related to the increasing influence of gravity as spreadings advance are poorly evidenced by the usually reported logarithm representation of x_f vs t. Rather than a well defined flexion point as seen in Fig. 4(a), the experimental curves reveal only a trend towards a slight increase of the slopes from values near $0.100 - 0.110$ to $0.125 - 0.135$ as the ratio x_f/a increases. In Fig. 5 we resume points from previously reported measurements [11] and from the experiments of this work (Fig. 6), which we shall refer to below. In Table III we give also the slopes of reported logarithmic curves x_f vs t for the whole experimental range, together with the values obtained in our experiments; in all the cases we give the corresponding range x_f/a. Unfortunately, these slopes are unavoidably affected by a dispersion comparable to the expected variation (0.106–0.135) because they are obtained from small intervals of x_f's values. Furthermore, a conceptual weakness results from the fact that they involve an averaging process. Therefore, though the agreement with the general trends and the typical values given by the theory is fairly good, we conclude that the results concerning the dependence x_f vs t provide only a qualitative noncritical test.

The magnitudes related to the thickness profile provide a much better test of the model. As shown in Figs. 4(c) and 4(d), both I and H_i' vary strongly across the transition; as an additional advantage, they may be directly obtained without the need of a time averaging process. However, their determination requires not only the knowledge of $x_f(t)$, but also the accurate measure-

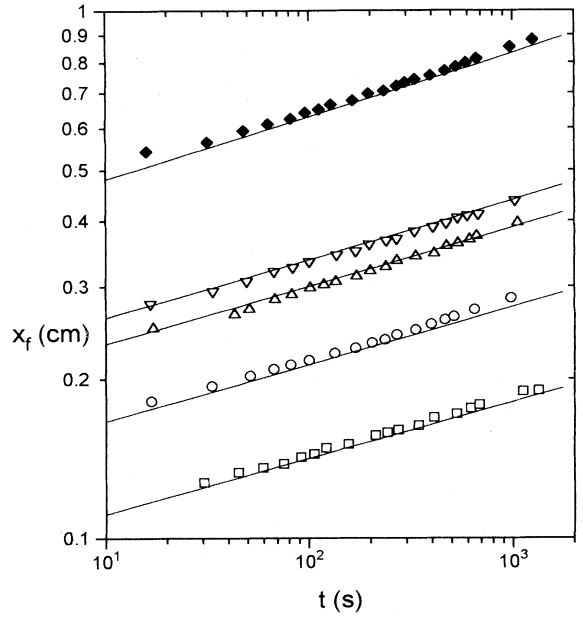

FIG. 5. Front positions x_f for five drops of different volumes ($\mu = 10$ P, $\gamma = 20.9$ dyn/cm) reported by Cazabat and Cohen-Stuart [11]: $V = 0.35$ 1.35, 4.03, 5.80, and 37.9 mm^3. The solid lines correspond to the quasi-self-similar solution for $\lambda = 10^{-6}$ cm.

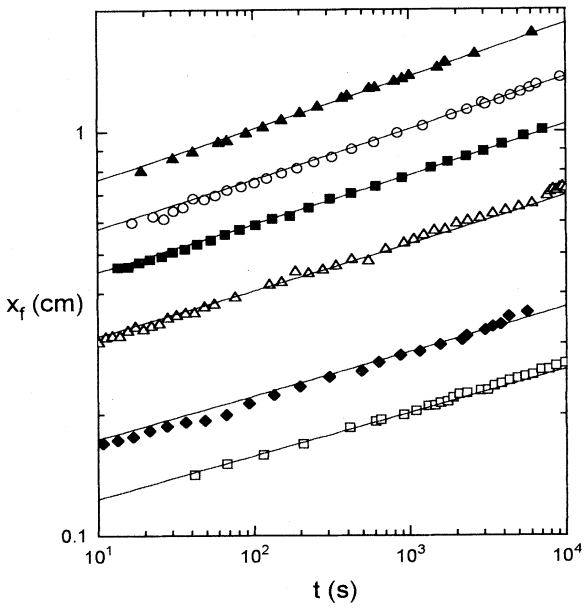

FIG. 6. Front positions for six drops of different volumes ($\mu = 10.3$ P, $\gamma = 20.9$ dyn/cm) from the present work: $V = 0.51$, 1.52, 10.32, 31.52, 65.36, and 144.3 mm^3. The solid lines correspond to the quasi-self-similar solution for $\lambda = 10^{-6}$ cm.

TABLE III. Experimental results for silicone oils (PDMS) on glass. The exponents p were calculated for the whole range of each experiment.

Reference	V (mm^3)	x_f/a interval	p ($x_f \approx t^p$)
[4] (μ = 10.8 and 130 P)	1.33–505	1.00–2.87	0.106–0.112
[11] (μ = 10 P)	0.35	0.85–1.26	0.109
	1.35	1.21–1.90	0.110
	4.03	1.67–2.64	0.116
	5.80	1.85–2.91	0.111
	37.9	3.60–5.89	0.116
[6] (μ = 1.95 P)	0.034–0.305	0.41–1.00	0.080–0.123
[21] (μ = 1.25 P)	1.02–38.4	1.67–7.33	0.129
Present work	0.51	0.96–1.80	0.112
(μ = 10.3 P)	1.52	1.14–2.42	0.119
	10.32	2.03–4.85	0.125
	31.52	3.12–6.73	0.125
	65.32	6.67–11.74	0.131
	144.3	5.37–11.74	0.134

ment of the volume V and $h_0(t)$, a magnitude that has received relatively scarce attention before. Likewise, to obtain $H_i'(t)$, the apparent contact angle $\theta_i(t)$ should be measured by means of specific techniques. Even if some of these measurements have been performed in several previous experiments, there is a lack of simultaneous accurate determinations of $x_f(t)$, $h_0(t)$, V, and $\theta_i(t)$. Besides, the reported values of I falling within the range of interest [12] are in agreement with the present model, but they are too few to give it definite support.

Therefore, we perform experiments for a wide range of volumes, from "light" drops ($V \cong 1\ mm^3$) to relatively "heavy" drops ($V \cong 100$ mm^3) of polydimethilsyloxane (PDMS). We use a Mach-Zehnder interferometer, with the substrate (glass) supporting the spreading drop placed in one of its arms (see Fig. 7). We determine $x_f(t)$, $h_0(t)$, and $h(x,t)$ from one of the interferometer arms [29]. The integration of the thickness profile provides an accurate value of the drop volume. The size of the Fraunhaufer diffraction pattern of the drop [30], formed by the second interferometer output, gives the ap-

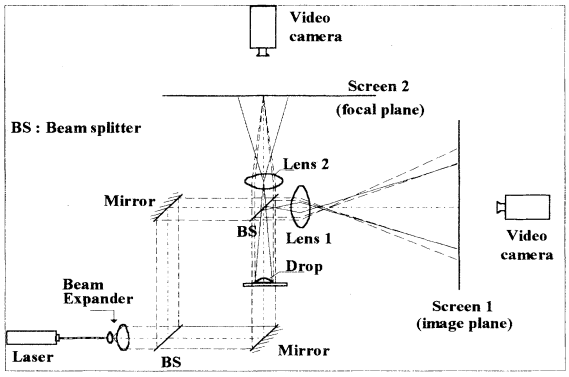

FIG. 7. Optical arrangement based on a Mach-Zehnder interferometer with outputs 1 and 2. The measurement of $h(x,t)$ is from the interferogram formed on screen 1, due to the superposition of the magnified image of the drop and a uniform light field. The drop image is formed by the beams coming from the bottom and the right-hand side of the interferometer. The measurement of $\theta_i(t)$ is from the far field diffraction pattern of the drop on screen 2.

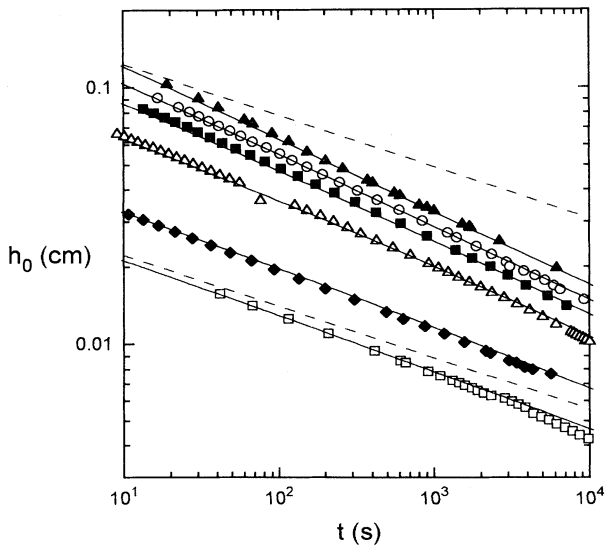

FIG. 8. Thickness at the center of the drop h_0 for the cases of Fig. 6. For comparison we include two straight dashed lines with slope -0.2, which is the exponent corresponding to an eventual, strict self-similar solution in the Laplace regime.

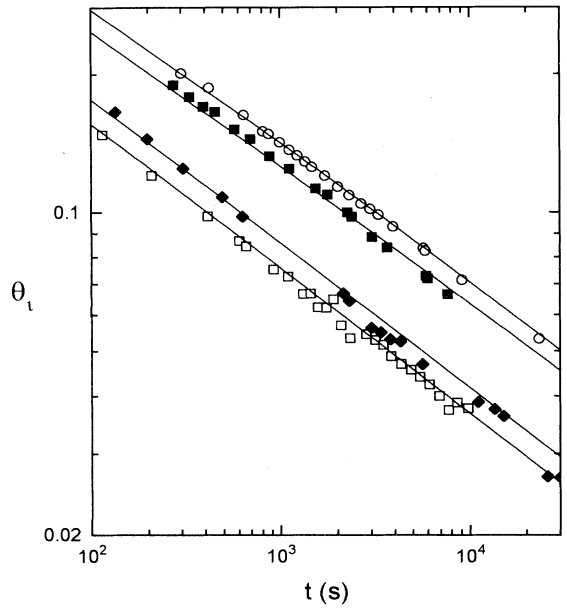

FIG. 9. Apparent contact angles for the cases of Fig. 6 in which θ_i was measured: $V = 0.51$, 1.52, 31.52, and 65.36 mm^3. The solid lines correspond to the quasi-self-similar solution for $\lambda = 10^{-6}$ cm.

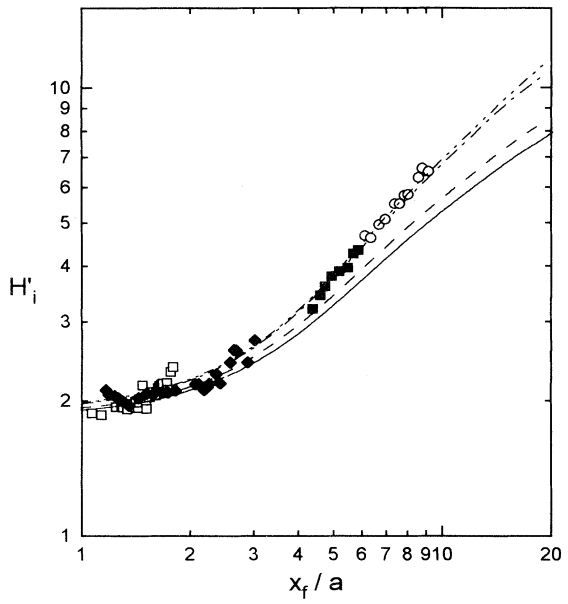

FIG. 11. Ratio between the apparent contact angle and the aspect ratio $H_i' = \tan\theta_i/(h_0/x_f)$ for the cases of Fig. 9 (symbols). The curves correspond to the quasi-self-similar solution for $\lambda = 10^{-6}$ cm: $V = 0.51$ mm^3 (solid curve), 1.52 mm^3 (dashed curve), 31.52 mm^3 (dash-dotted curve), and 65.36 mm^3 (dash–double-dotted curve).

parent contact angle. Both patterns are simultaneously recorded by video cameras.

In Figs. 8 and 9 we compare the experimental values (symbols) of $h_0(t)$ and $\theta_i(t)$ with the theory (solid lines). In order to visualize the departure from strict self-similarity we have added in Fig. 8 two straight lines of slope -0.2, which is the exponent corresponding to an eventual strict self-similar solution in the Laplace regime. It can be seen that, as expected, the departures are larger for higher volumes. Similar but smaller departures could be also observed for $\theta_i(t)$ in Fig. 9. The agreement is satisfactory, except for the case $V = 0.51$ mm^3 in Fig. 8, where there appears a departure from the model solution for very small thicknesses (≤ 50 μm). From the data reported in Figs. 6, 8, and 9 it is possible to determine I and H_i', which are shown in Figs. 10 and 11 together with the corresponding theoretical curves. In Fig. 10 we have added data reported elsewhere [12] (stars). Despite the dispersion due to the error accumulation from the values of x_f, h_0, θ_i, and V, the general agreement with the predictions of the model is remarkably good.

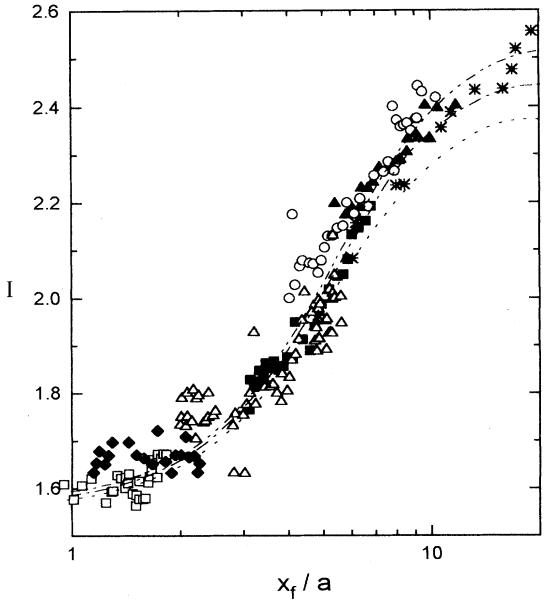

FIG. 10. Volumetric shape factors I for the cases of Fig. 6. The lines correspond to the quasi-self-similar solution for some of the volumes: $V = 1$ mm^3 (dotted curve), 10 mm^3 (dash-dotted curve), and 100 mm^3 (dash–double-dotted curve). The stars [12] correspond to $V = 200$ mm^3.

The curves $x_f(t)$, $h_0(t)$, and, as a consequence, $I(x_f/a)$ are not very sensitive to the choice of λ. In practice, a change by a factor 2 or 3 does not produce appreciable differences, so that only the order of magnitude of λ ($\approx 10^{-6}$ cm) is suggested. However, $\theta_i(t)$ and H_i' are much more sensitive to λ, perhaps because the inflection point is very close the front itself. Therefore, we calculate the best-fitting value of λ from the θ_i data. In our experiments (PDMS with viscosity $\mu = 10$ P on a glass substrate), we get $\lambda = (1 \pm 0.1) \times 10^{-6}$ cm.

V. CONCLUDING REMARKS

A quasi-self-similar solution may be properly used to describe the spreading of liquid drops driven by both

gravity and Laplace pressure under the condition of complete wetting. The solution results from the addition of successive self-similar solutions, each one corresponding to the instantaneous values of the fractional slipping length Λ and the Bond number B. This approach does not need spatial matching because each one of the time added solutions is completely determined from the center to the periphery. The main assumption is that the spatial averaged horizontal velocity is always linear on the coordinate in the flow direction. Even though we do not attempt to demonstrate the mathematical conditions for the validity of the approach, its applicability is clearly related with the smallness of the diffusion time of the velocity field with respect to the time evolution of the system.

We wish to point out that the quasi-self-similar approach can also be used in connection with hypotheses other than the relaxation of the no-slip condition. In fact, in a previous work [15] we used this method together with a quite different way of dealing with the front condition for spreadings where the Laplace pressure was the only driving force.

Quasi-self-similarity appears as an analog of quasiequilibrium, in the sense that the evolution of a system is described as a succession of "self-similar states," just as the evolution is a succession of "equilibrium states" in the latter case. The most significant difference is that no additional hypothesis for the spreading rate is needed since it is automatically provided by the instantaneous self-similar profile. In general, we believe that the quasi-self-similar method proposed here can be useful for cases where strict self-similarity does not hold, but in which the time of adjustment of the system to changes of the governing parameters is much smaller than the characteristic times of their variation. Therefore, the essential features of the intermediate asymptotic behavior are retained.

ACKNOWLEDGMENTS

This work was supported by the Consejo Nacional de Investigaciones Científicas y Técnicas, Comisión de Investigaciones Científicas de la Provincia de Buenos Aires, and Universidad Nacional del Centro de la Provincia de Buenos Aires.

[1] H.E. Huppert, J. Fluid Mech. **121**, 43 (1982).
[2] J. Gratton and F. Minotti, J. Fluid Mech. **210**, 155 (1990).
[3] J. Lopez, C.A. Miller, and E. Ruckenstein, J. Colloid Interface Sci. **53**, 460 (1976).
[4] L.H. Tanner, J. Phys. D **12**, 1473 (1979).
[5] V.M. Starov, Colloid J. USSR **45**, 1009 (1983).
[6] J.D. Chen, J. Colloid Interface Sci. **122**, 60 (1988).
[7] J.D. Chen and N. Wada, Phys. Rev. Lett. **62**, 3050 (1989).
[8] J.D. Chen and N. Wada, J. Colloid Interface Sci. **148**, 207 (1992).
[9] J.A. Diez, R. Gratton, L.P. Thomas, and B. Marino, Phys. Fluids A **6**, 24 (1994).
[10] P. Levinson, A.M. Cazabat, M.A. Cohen Stuart, F. Heslot, and S. Nicolet, Rev. Phys. Appl. **23**, 1009 (1988).
[11] A.M. Cazabat and M.A. Cohen Stuart, J. Phys. Chem. **90**, 5845 (1986); see also A.M. Cazabat and M.A. Cohen Stuart, Phys. Chem. Hydrodynamics **9**, 23 (1987).
[12] F. Brochard-Wyart, H. Hervet, C. Redon, and F. Rondelez, J. Colloid Interface Sci. **142**, 518 (1991); C. Redon, Ph.D. thesis, Université de Paris VI, 1991 (unpublished).
[13] M. Brenner and A. Bertozzi, Phys. Rev. Lett. **71**, 593 (1993).
[14] B. Marino, L.P. Thomas, J. Diez, and R. Gratton, J. Colloid Interface Sci. **177**, 14 (1996).
[15] J.A. Diez, R. Gratton, L.P. Thomas, and B. Marino, J. Colloid Interface Sci. **168**, 15 (1994).
[16] L.M. Hocking, J. Fluid Mech. **79**, 209 (1977).
[17] L.M. Hocking and A.D. Rivers, J. Fluid Mech. **121**, 425 (1982).
[18] L.M. Hocking, Q. J. Mech. Appl. Math **36**, 55 (1983).
[19] L.M. Hocking, J. Fluid Mech. **239**, 671 (1992).
[20] P. Ehrhard and S.H. Davis, J. Fluid Mech. **229**, 365 (1991).
[21] P. Ehrhard, J. Fluid Mech. **257**, 463 (1993).
[22] E.B. Dussan V., J. Fluid Mech. **77**, 665 (1976).
[23] R.G. Cox, J. Fluid Mech. **168**, 169 (1986).
[24] H.P. Greenspan, J. Fluid Mech. **84**, 125 (1978).
[25] E.B. Dussan V., E. Ram, and S. Garoff, J. Fluid Mech. **230**, 97 (1991).
[26] P.G. de Gennes, Rev. Mod. Phys. **57**, 827 (1985).
[27] E. M. Sparrow, H. Quack, and C. J. Boerner, AIAA J. **8**, 1936 (1970).
[28] L. Dresner, *Similarity Solutions of Nonlinear Partial Differential Equations* (Pitman, New York, 1983).
[29] W. Merzkirch, *Flow Visualization*, 2nd ed. (Academic, London, 1987).
[30] C. Allain, D. Auserré, and F. Rondelez, J. Colloid Interface Sci. **107**, 5 (1985).